JACS
JOURNAL OF THE AMERICAN CHEMICAL SOCIETY
pubs.acs.org/JACS
Article

Imaging of Chemical Kinetics at the Water–Water Interface in a Free-Flowing Liquid Flat-Jet

H. Christian Schewe,[#] Bruno Credidio,[#] Aaron M. Ghrist,[#] Sebastian Malerz, Christian Ozga, André Knie, Henrik Haak, Gerard Meijer, Bernd Winter, and Andreas Osterwalder*

Cite This: J. Am. Chem. Soc. 2022, 144, 7790–7795
Read Online
ACCESS | Metrics & More | Article Recommendations | Supporting Information

ABSTRACT: We present chemical kinetics measurements of the luminol oxidation chemiluminescence (CL) reaction at the interface between two aqueous solutions, using liquid jet technology. Free-flowing liquid microjets are a relatively recent development that have found their way into a growing number of applications in spectroscopy and dynamics. A variant thereof, called flat-jet, is obtained when two cylindrical jets of a liquid are crossed, leading to a chain of planar leaf-shaped structures of the flowing liquid. We here show that in the first leaf of this chain, the fluids do not exhibit turbulent mixing, providing a clean interface between the liquids from the impinging jets. We also show, using the example of the luminol CL reaction, how this setup can be used to obtain kinetics information from friction-less flow and by circumventing the requirement for rapid mixing by intentionally suppressing all turbulent mixing and instead relying on diffusion.

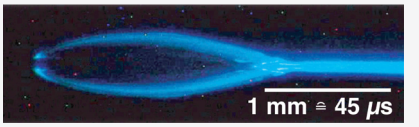

INTRODUCTION

Fast-flowing liquid microjets are a powerful tool for the preparation of volatile liquids, including water, even in high-vacuum environments.[1−5] They recently gained much interest in particular for in-vacuum applications, where the jet travels freely for some millimeters before decaying into droplets and freezing. One of the prime factors that make them interesting tools is the free flow through air or vacuum, which permits unobstructed optical access to a liquid and thus enables a wide range of spectroscopic detections that are incompatible with many solid container materials. Recent applications include X-ray photoelectron spectroscopy,[1,6−14] evaporation dynamics,[15−21] attosecond-pulse generation,[22,23] and liquid–gas scattering.[24,24,25] The most common implementation is a single cylindrical jet, obtained by forcing a liquid at a pressure of a few bars through a 10−50 μm-diameter nozzle, which results in a laminar jet with a flow velocity of tens of m/s.

Many experiments demand a planar surface in order to avoid unwanted averaging over effects resulting from the angle-dependent surface normal.[24,26] Different arrangements exist to produce laminar-flow planar surfaces,[27,28] among which a widely used setup is the crossing and impinging of two cylindrical jets.[29] For a large enough Reynolds number, this produces a chain of few-micron-thin leaf-shaped sheets, each bound by a relatively thick fluid rim and stabilized by an interplay of surface tension and fluid inertia. More specifically, at the crossing point of the two cylindrical jets, the aqueous solution is pushed outwards, continuing to move in an overall forward direction. However, this outward motion is counteracted by the solutions' surface tension, such that after some distance the outer boundaries of this structure merge. The resulting flow leads to a fluid chain of mutually orthogonal, thin, linked, and stable leaf-shaped sheets bound by relatively thick fluid rims, each providing a planar water surface.[30] Individual links in the chain decrease successively in size until the chain coalesces into a cylindrical stream through the action of viscosity. Whether or not stable sheets can be generated, or sheets rather destabilize, break, or disintegrates into a spray of droplets is governed by surface tension, viscous, inertial, and aerodynamic forces.[31] Consecutive sheet planes are perpendicular to each other. The stability and geometry of this structure are governed by solution properties such as surface tension and viscosity and by controlled parameters such as the flow rate and jet diameter.[29,31] An important question about such objects is whether the first leaf of the chain contains a turbulent mixture of the fluids from the two jets or if these flow alongside each other, yet we are not aware of any experimental study addressing this question. Indeed, the second option implies that a well-defined liquid–liquid interface is generated, which is of great interest in the case of two different solvents but also for identical solvents of different compositions. Previous studies have shown that in microfluidic devices, it is possible to prepare well-defined interfaces between miscible and immiscible fluids by keeping the liquid flow laminar, and these devices have been used in studies targeting structural and dynamical aspects of interfaces.[32,33] In contrast to free-flowing flat-jets, microfluidics inherently require a container material which, on the one hand, imposes limitations on the systems in terms of flow dynamics, because friction on the walls leads to

Received: January 31, 2022
Published: April 26, 2022

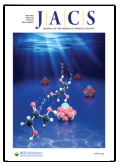

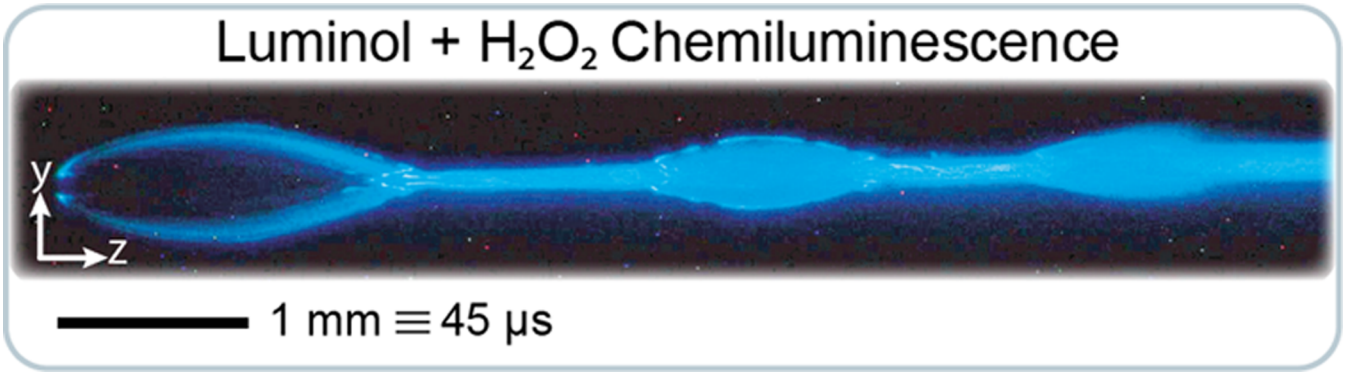

Figure 1. Photograph of a water flat-jet glowing blue as a result of chemiluminescence.

modified flow patterns, and on the available spectroscopic tools, on the other hand, because the container material itself absorbs electromagnetic radiation in ranges that may be critical for the system under investigation.

We here demonstrate that impinging, but free-flowing, jets do produce a leaf structure, where the fluids flow alongside each other in the first leaf and thus represent a tool to gain access to the liquid−liquid interface of miscible fluids. This finding demonstrates an important aspect of free-flowing microjets, which makes them a powerful borderless alternative to microfluidics and opens the door toward the investigation of chemical reactions and in-vacuum studies at liquid−liquid interfaces, with the option of using extreme ultraviolet and X-ray radiation that is only limited by the absorption spectrum of the solvent itself. Species in either solution diffuse across the interface while flowing downstream, thereby creating a steady-state system with an increasingly overlapping region, where chemical reactions can take place. Based on this, here, we also demonstrate a technique for chemical kinetics studies under completely controlled conditions, which explicitly avoids the necessity for rapid mixing and benefits from the free-flowing jets that are not perturbed by friction on container walls.[34] By combining two jets with different reactants and applying a suitable spectroscopic detection scheme, the flow axis of the jet represents the time to see and image directly the progress of the reaction. Typical leaf surface dimensions are 1.5 mm × 0.5 mm with flow velocities of a few 10 m/s corresponding to a flow time through the first leaf of around 50−100 μs, thus covering a time scale for chemical kinetics that currently is difficult to access by other methods. Indeed, conventional stopped-flow techniques are best suited for studies on time scales around a millisecond, while laser-induced techniques work best on faster time scales.

The present experiment detects photons from a chemiluminescence (CL) reaction, allowing at the same time the proof for the controlled formation of the liquid−liquid interface and the imaging of the chemical reaction kinetics. Our sample reaction is the oxidation of 5-amino-2,3-dihydro-1,4-phthalazinedione, known as luminol, which is oxidized by H_2O_2 in the presence of a transition metal ion.[35,36] The reaction product is an electronically excited state of deprotonated 3-aminophthalic acid (AP*), which relaxes to the electronic ground state by emitting a blue photon.[37−39] This reaction is thus well suited for the main purpose of the present study, fulfilling the requirements of being straightforward to prepare, sufficiently fast to be observed here, and detectable with a common camera setup.

Injecting the principal reactants through individual jets yields a liquid flat-jet that luminesces exclusively where the liquids mix. Figure 1 is the resulting photograph of the glowing flat-jet, where the cylindrical jets enter from the left and flow to the right. Such an image provides a direct visualization of the dynamics in the flat-jet: from the intensity distribution of the emitted light, we can immediately conclude that there is no turbulent mixing in the flat region of the first leaf and infer information on the kinetics. Complete mixing of the solutions leads to a uniform blue glow as it is observed in rims and onward from the second leaf. However, the first leaf displays a gradual increase of the luminescence, indicative of diffusion across the well-defined interface and determined by the relative rates of diffusion, chemical reaction kinetics, and luminescence. The luminol−H_2O_2 reaction has been found to be sufficiently fast to yield diffusion-limited reaction kinetics in the present setup. Our imaging setup allows for a time resolution of around 2 μs, and as shown in the Supporting Information, on this time scale the reaction takes place instantaneously. This system is thus ideally suited for spatial mapping of solution mixing and the demonstration of the feasibility of reaction kinetics measurements.

EXPERIMENTAL SECTION

In the present experiment, described in detail in the Supporting Information, we generate the flat-jet by colliding two liquid jets in atmosphere, one containing an aqueous H_2O_2 solution, and the other containing luminol and copper ions. More details on the experimental setup, and a computer rendering of the mounted capillaries, are provided in Figure SI-2 of the Supporting Information

A photograph of a typical flat-jet, but with no chemical reaction, used in the present experiments is shown in Figure 2A. Rims and turnover point to the second leaf are clearly visible. Color structures on the leaf surface are optical interferences resulting from the sample illumination. Figure 2B shows a cross section of the flat-jet in the plane of the two original jets, sketching the merged structure formed by the two flat-jets of solutions #1 and #2, joined by the interface. Here, the two cylindrical jets are represented by the two arrows crossing at angle α. The downstream increase of the interfacial layer thickness, indicated as the dark blue area, results from diffusion of species across the boundary (see the Supporting Information for calculations of the resulting concentration distributions).

RESULTS AND DISCUSSION

Figure 3A shows a false-color plot of the CL intensity in the $y - z$ plane, from the first leaf in Figure 1, with the camera oriented along the x-axis (see Figure 2B). Two 50 μm jets enter from the left, in the $x - z$ plane. The first leaf in this arrangement has dimensions of l = 1.5 mm and w = 0.3 mm,

https://doi.org/10.1021/jacs.2c01232
J. Am. Chem. Soc. 2022, 144, 7790−7795

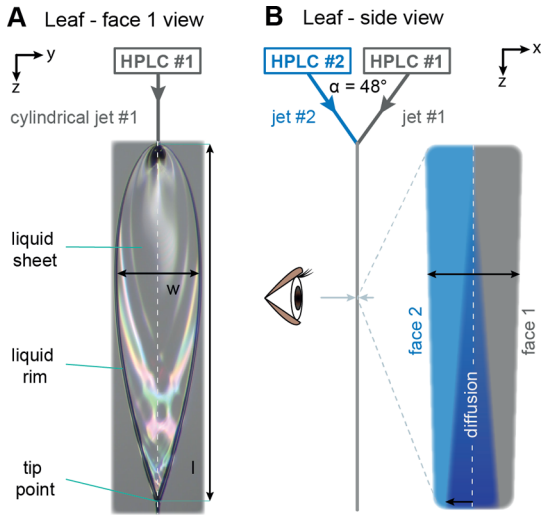

Figure 2. Experimental arrangement to generate the flat-jet. Two cylindrical liquid microjets, operated by separate HPLC pumps, are crossed at an angle of $\alpha = 48°$. One contains a luminol solution and Cu^{2+} ions, the second an aqueous H_2O_2. (A) View at the face of the first leaf. The plane spanned by the two cylindrical jets is vertical to the leaf plane. This image was taken with pure water and no chemical reaction. (B) Sketch showing the geometry used for CL detection and a cross section of the first leaf. A CCD camera faces the leaf surface and collects the CL.

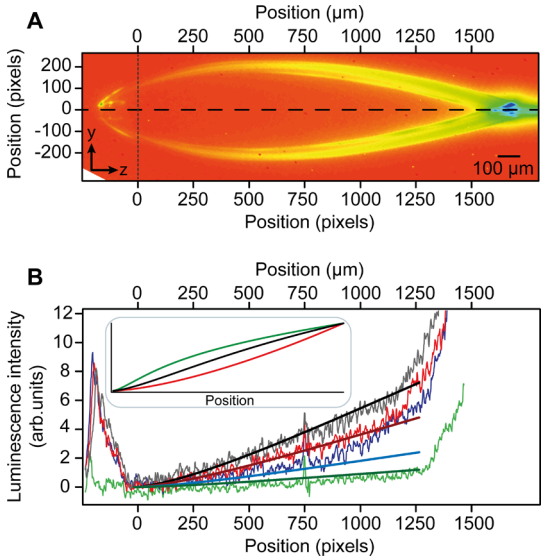

Figure 3. (A) False-color image of the measured CL intensity within the first leaf of the flat-jet (blue is high intensity; red is zero intensity). (B) CL signal intensity along the z-direction at $y = 0$, indicated by the dashed horizontal line in A, for luminol concentrations of 6 g/L (black line), 4 g/L (red line), 2 g/L (blue line), and 1 g/L (green line), respectively. Thick solid lines are numerical results. Inset: calculated results for cases with extreme (red and green) ratios and the results found here (black) between reaction and diffusion rates.

respectively, and a flow speed of 23 m/s. They are not visible because no luminescence is emitted from the individual reactant jets, which impinge at around $z = -100 \pm 100$ pixels and $y = 0 \pm 50$ pixels. Calibration of the pixel scale and conversion to the μm scale at the top is obtained using the known cylindrical-jet diameter in Figure 2A. The flat-jet origin is defined as the point where a laminar flat-jet forms and CL starts to be observable. CL intensity at negative z values and in the rims mirrors the turbulences in those regions. Here, the observed relative signal increase along the flow is due to the fact that for small z-values, less liquid accumulates in the rims. Mixing in this region is likely by turbulences but possibly also involving complex surface migrations. In contrast, in the flat region only a slight intensity increase, starting at zero luminescence, is observed along the flow direction. The specific form of this increase is defined by the overall dynamics of the process and is used to extract information on the rates of the involved processes. The CL intensity as a function of the downstream coordinate (along the z-axis at $y = 0$; dashed line in Figure 3A) is shown in Figure 3B. Results are plotted for four different solutions with luminol concentrations of 6 g/L (grey), 4 g/L (red), 2 g/L (blue), and 1 g/L (green), respectively (all other reactants in this solution are scaled accordingly). These graphs, along with Figures 1 and 3A, reveal the following: (1) all leaves except the first one exhibit uniform CL intensity of similar magnitude in the flat parts and in the rims, indicating complete mixing of the two liquids. (2) The CL intensity observed at $z < 0$ first decreases to zero before gradually increasing. (3) The CL intensity in the first leaf increases toward positive z, supporting the assumption of reagent diffusion across the interface. Point 2 is an important confirmation that the CL reaction, including the final luminescence step, proceeds fast on the time scale in comparison with flow speed, diffusion, and reaction kinetics, and that at the origin a purely laminar flow is established (also see the Supporting Information). We note that the luminescence lifetime of AP* is not known precisely, and a measurement through, for example, excitation with a short laser pulse and monitoring of the luminescence would be of high interest. However, such a study is beyond the scope of the present work.

The overall kinetics are assessed by theoretically reproducing the measured CL profiles of Figure 3B, using a simple kinetics model that includes the diffusion, the principal reaction steps (detailed in the Supporting Information), and luminescence. The photon flux Φ from CL results from the decay of AP*

$$\Phi = k_P[AP^*](t) \quad (1)$$

where k_P is the rate coefficient for CL and $[AP^*](t)$ is the time-dependent product concentration. AP* is formed in a series of chemical reactions outlined in the Supporting Information.[35,38,40−42] The rate of this process can be written as a function of the limiting reactant concentrations

$$d[AP^*]/dt = k_R[H_2O_2][LH^-] \quad (2)$$

where k_R is a collective rate coefficient for the chemical reaction sequence that incorporates the various steps leading to AP*. The required high pH of the luminol solution indicates that it is present exclusively in the deprotonated form LH^-, conditions that have been found to be favorable for the reaction.[43,44]

Applying the coordinate system introduced in Figures 2 and 3A, the relevant spatial dimensions thus are both the z-axis (which translates into a time axis, t) and the x-coordinate perpendicular to the leaf surface, which is the principal direction of diffusion and hence mixing of the reactants. The concentration distribution $c(x, t)$ is derived from the initial concentrations, c_0, using Fick's law.[45] In the model of the two-solution flat-jet, the initial concentration distributions, $c(x = 0, t = 0)$, are step-functions, where the concentration of either

https://doi.org/10.1021/jacs.2c01232
J. Am. Chem. Soc. 2022, 144, 7790−7795

reactant is c_0 on its original side and zero elsewhere. As time progresses, the diffusion-determined profile for each species i is described by an error-function Γ

$$c_i(x, t) = \frac{c_{0,i}}{2}\left\{1 - \Gamma\left(\frac{x}{2\sqrt{D_i t}}\right)\right\} \tag{3}$$

where D_i is the diffusion coefficient for species i and t is the time, which is defined by the flow velocity v and the position along the jet propagation as $t = z/v$. As the reaction progresses, the reactants are consumed, and this is taken into account globally by adjusting $c_{0,i}$ for both species after each time step by the amount of products that have been formed. Through this approximation, we explicitly take into account minor changes of both reactant concentrations and assume that the reaction happens uniformly across the entire interface.

In a second step, the concentration profiles from eq 3, expressed as a function of z, are convolved with each other and fed into eq 2, thus incorporating diffusion into the kinetic model. This yields the final profile for [AP*] along the z axis, and eq 1 is then used to calculate the CL intensity

$$\frac{\Delta[\mathrm{AP}^*]}{\Delta z} = \frac{1}{v}[-k_\mathrm{p}[\mathrm{AP}^*] + k_\mathrm{R}\Omega(z)] \tag{4}$$

here, $\Omega(z)$ is the integral along z of the convoluted concentration profiles along x, and it thus accounts for the widening of the interface downstream in the jet (see the Supporting Information). The terms in brackets are the rate of decrease of [AP*] due to CL, in accordance with eq 1, and of increase due to the chemical reaction, eq 2.

The resulting expression is then numerically integrated to yield synthetic luminescence traces along the jet axis, and rate coefficients are fitted to reproduce the experimental results from Figure 3B, as is shown by thick solid lines in the same graph. In the current proof-of-principle study, we are not able to extract absolute rate coefficients because some of the rates are correlated and because in this case a calibration of the luminescence measurement was not attempted. Here, we present a simplified analysis that reproduces the shape of the traces that depends on the relative magnitudes of the rates of diffusion, luminescence, and chemical kinetics. In the Supporting Information, we elaborate on a procedure that will enable a quantitative analysis for future experiments, where a calibration will be included.

From the results in Figure 3B, we extract the following: the interplay and relative magnitudes of diffusion, reaction kinetics, and fluorescence rates determine the overall magnitude of the CL signal but in particular also the profile of the intensity along the z axis. The global shape of the curve is an asymmetric sigmoidal evolution, and depending on the relative magnitudes of the different rates, we probe different parts of that curve, as shown in the inset of Figure 3B. The curve starts with a positive curvature, which is emphasized in the red curve, where we artificially reduced the diffusion coefficients. It converges, showing a negative curvature, on a threshold, as is clearly seen in the green curve, where we artificially slowed down the luminescence. The intermediate regime, shown in black, provides a near-linear evolution as is also observed experimentally. Interestingly, the reaction rate coefficient itself merely leads to an overall scaling of the signal but without affecting the shape, thus underlining that for a qualitative understanding, calibrated measurements seem unimportant: even without it, the shape of the curve reveals principal aspects of the dominating kinetics. The curvature also does not depend on the concentrations, and nearly identical results to those shown in Figure 3 are obtained by linearly scaling a single calculation with concentration.

CONCLUSIONS

A free-flowing liquid flat-jet has been produced from two different solutions to form a controlled liquid−liquid interface with uninhibited optical access from both sides. Using the CL reaction of luminol-oxidation by H_2O_2, we created a marker for the temporal evolution of the mixing in the interfacial layer. By measuring the CL intensity distribution from the surface of the first leaf, we demonstrate that the individual cylindrical jets merge into a laminar regime, and mixing between the two solutions within this leaf happens solely due to diffusion. We further show that the obtained CL image reveals reaction kinetics on the sub-ms timescale. We observe a linear dependence of CL on reactant concentrations, indicative of first order kinetics in the rate-limiting substances. By modeling the experimental data theoretically, and by including diffusion, chemical kinetics, and luminescence, we were able to qualitatively replicate the quasilinear increase of the CL intensities measured experimentally as well as to quantitatively reproduce the concentration dependence.

This study demonstrates the potential buried in the free-flowing flat-jet technology for the investigation of liquid−liquid interfaces and interfacial chemical reactions for identical solvents. The flat-jet represents a steady-state system, wherein the time axis is transformed into a spatial coordinate, and imaging provides direct access to time-dependent phenomena. In contrast to otherwise equivalent experiments using microfluidics, free-flowing jets are not limited by the presence of containers. These affect the flow dynamics and impose restrictions on the range of wavelengths applicable to spectroscopic studies. Investigations of liquid−liquid interfaces using free-flowing fluids on the other hand can be extended to X-ray spectroscopies on vacuum flat-jets to access electronic structure, exploiting the unique element specificity and sensitivity to chemical environment of these techniques, and the controlled preparation of interfaces now offers possibilities for the study of, for example, transfer processes, chemical dynamics, or catalysis.

ASSOCIATED CONTENT

Supporting Information

The Supporting Information is available free of charge at https://pubs.acs.org/doi/10.1021/jacs.2c01232.

Details of the target reaction, experimental setup, luminescence lifetime, as well as additional information on the calculation of concentration gradients and kinetics, and an alternative mathematical approach to fit the experimental results to extract quantitative information (PDF)

AUTHOR INFORMATION

Corresponding Author

Andreas Osterwalder − *Institute for Chemical Sciences and Engineering (ISIC), Ecole Polytechnique Fédérale de Lausanne (EPFL), 1015 Lausanne, Switzerland;* orcid.org/0000-0001-7346-4808; Email: andreas.osterwalder@epfl.ch

https://doi.org/10.1021/jacs.2c01232
J. Am. Chem. Soc. 2022, 144, 7790−7795

Authors

H. Christian Schewe − *Fritz-Haber-Institut der Max-Planck-Gesellschaft, 14195 Berlin, Germany; Institute of Organic Chemistry and Biochemistry, Czech Academy of Sciences, 16610 Prague 6, Czech Republic;* orcid.org/0000-0003-3232-5486

Bruno Credidio − *Institute for Chemical Sciences and Engineering (ISIC), Ecole Polytechnique Fédérale de Lausanne (EPFL), 1015 Lausanne, Switzerland*

Aaron M. Ghrist − *Fritz-Haber-Institut der Max-Planck-Gesellschaft, 14195 Berlin, Germany; Department of Chemistry, University of Southern California, Los Angeles, California 90089-0482, United States;* orcid.org/0000-0003-2196-9278

Sebastian Malerz − *Fritz-Haber-Institut der Max-Planck-Gesellschaft, 14195 Berlin, Germany;* orcid.org/0000-0001-9570-3494

Christian Ozga − *Institut für Physik und CINSaT, Universität Kassel, 34132 Kassel, Germany*

André Knie − *Institut für Physik und CINSaT, Universität Kassel, 34132 Kassel, Germany;* orcid.org/0000-0002-2208-8838

Henrik Haak − *Fritz-Haber-Institut der Max-Planck-Gesellschaft, 14195 Berlin, Germany*

Gerard Meijer − *Fritz-Haber-Institut der Max-Planck-Gesellschaft, 14195 Berlin, Germany;* orcid.org/0000-0001-9669-8340

Bernd Winter − *Fritz-Haber-Institut der Max-Planck-Gesellschaft, 14195 Berlin, Germany;* orcid.org/0000-0002-5597-8888

Complete contact information is available at: https://pubs.acs.org/10.1021/jacs.2c01232

Author Contributions

#H.C.S., B.C., and A.M.G. contributed equally

Notes

The authors declare no competing financial interest.

■ ACKNOWLEDGMENTS

This work was funded by the SNF (project 200021E-171721), the DFG in the context of a D-A-CH collaboration, and by the EPFL-MPG doctoral school. We thank Marco Picasso and François Gallaire (both EPFL) for useful discussions.

■ REFERENCES

(1) Faubel, M. *Photoionization and Photodetachment*; Advanced Series in Physical Chemistry; World Scientific, 2000; Vol. *10*; pp 634−690.

(2) Faubel, M.; Steiner, B.; Toennies, J. P. Photoelectron Spectroscopy of Liquid Water, Some Alcohols, and Pure Nonane in Free Micro Jets. *J. Chem. Phys.* **1997**, *106*, 9013−9031.

(3) Faubel, M.; Siefermann, K. R.; Liu, Y.; Abel, B. Ultrafast Soft X-Ray Photoelectron Spectroscopy at Liquid Water Microjets. *Acc. Chem. Res.* **2012**, *45*, 120−130.

(4) Winter, B.; Faubel, M. Photoemission from Liquid Aqueous Solutions. *Chem. Rev.* **2006**, *106*, 1176−1211.

(5) Faubel, M.; Schlemmer, S.; Toennies, J. P. A Molecular Beam Study of the Evaporation of Water from a Liquid Jet. *Z. Phys. D: At., Mol. Clusters* **1988**, *10*, 269−277.

(6) Ali, H.; Seidel, R.; Bergmann, A.; Winter, B. Electronic Structure of Aqueous-Phase Anatase Titanium Dioxide Nanoparticles Probed by Liquid Jet Photoelectron Spectroscopy. *J. Mater. Chem. A* **2019**, *7*, 6665−6675.

(7) Buttersack, T.; Mason, P. E.; McMullen, R. S.; Martinek, T.; Brezina, K.; Hein, D.; Ali, H.; Kolbeck, C.; Schewe, C.; Malerz, S.; Winter, B.; Seidel, R.; Marsalek, O.; Jungwirth, P.; Bradforth, S. E. Valence and Core-Level X-Ray Photoelectron Spectroscopy of a Liquid Ammonia Microjet. *J. Am. Chem. Soc.* **2019**, *141*, 1838−1841.

(8) Fransson, T.; Harada, Y.; Kosugi, N.; Besley, N. A.; Winter, B.; Rehr, J. J.; Pettersson, L. G. M.; Nilsson, A. X-Ray and Electron Spectroscopy of Water. *Chem. Rev.* **2016**, *116*, 7551−7569.

(9) Jungwirth, P.; Winter, B. Ions at Aqueous Interfaces: From Water Surface to Hydrated Proteins. *Annu. Rev. Phys. Chem.* **2008**, *59*, 343−366.

(10) Lewis, T.; Faubel, M.; Winter, B.; Hemminger, J. C. CO2 Capture in Amine-Based Aqueous Solution: Role of the Gas-Solution Interface. *Angew. Chem., Int. Ed.* **2011**, *50*, 10178−10181.

(11) Winter, B. Liquid Microjet for Photoelectron Spectroscopy. *Nucl. Instrum. Methods Phys. Res., Sect. A* **2009**, *601*, 139−150.

(12) Karashima, S.; Yamamoto, Y.-i.; Suzuki, T. Ultrafast Internal Conversion and Solvation of Electrons in Water, Methanol, and Ethanol. *J. Phys. Chem. Lett.* **2019**, *10*, 4499−4504.

(13) Suzuki, T. Time-Resolved Photoelectron Spectroscopy of Non-Adiabatic Electronic Dynamics in Gas and Liquid Phases. *Int. Rev. Phys. Chem.* **2012**, *31*, 265−318.

(14) Suzuki, T. Ultrafast Photoelectron Spectroscopy of Aqueous Solutions. *J. Chem. Phys.* **2019**, *151*, 090901.

(15) Ryazanov, M.; Nesbitt, D. J. Quantum-State-Resolved Studies of Aqueous Evaporation Dynamics: NO Ejection from a Liquid Water Microjet. *J. Chem. Phys.* **2019**, *150*, 044201.

(16) Faust, J. A.; Sobyra, T. B.; Nathanson, G. M. Gas−Microjet Reactive Scattering: Collisions of HCl and DCl with Cool Salty Water. *J. Phys. Chem. Lett.* **2016**, *7*, 730−735.

(17) Hahn, C.; Kann, Z. R.; Faust, J. A.; Skinner, J. L.; Nathanson, G. M. Super-Maxwellian Helium Evaporation from Pure and Salty Water. *J. Chem. Phys.* **2016**, *144*, 044707.

(18) Lancaster, D. K.; Johnson, A. M.; Kappes, K.; Nathanson, G. M. Probing Gas−Liquid Interfacial Dynamics by Helium Evaporation from Hydrocarbon Liquids and Jet Fuels. *J. Phys. Chem. C* **2015**, *119*, 14613−14623.

(19) Sobyra, T. B.; Melvin, M. P.; Nathanson, G. M. Liquid Microjet Measurements of the Entry of Organic Acids and Bases into Salty Water. *J. Phys. Chem. C* **2017**, *121*, 20911−20924.

(20) Murdachaew, G.; Nathanson, G. M.; Halonen, L. Deprotonation of Formic Acid in Collisions with a Liquid Water Surface Studied by Molecular Dynamics and Metadynamics Simulations. *Phys. Chem. Chem. Phys.* **2016**, *18*, 29756−29770.

(21) Faust, J. A.; Nathanson, G. M. Microjets and Coated Wheels: Versatile Tools for Exploring Collisions and Reactions at Gas−Liquid Interfaces. *Chem. Soc. Rev.* **2016**, *45*, 3609−3620.

(22) Jordan, I.; Jain, A.; Gaumnitz, T.; Ma, J.; Wörner, H. J. Photoelectron Spectrometer for Liquid and Gas-Phase Attosecond Spectroscopy with Field-Free and Magnetic Bottle Operation Modes. *Rev. Sci. Instrum.* **2018**, *89*, 053103.

(23) Yin, Z.; Luu, T. T.; Wörner, H. J. Few-Cycle High-Harmonic Generation in Liquids: In-Operando Thickness Measurement of Flat Microjets. *J. Phys.: Photonics* **2020**, *2*, 044007.

(24) Lancaster, D. K.; Johnson, A. M.; Burden, D. K.; Wiens, J. P.; Nathanson, G. M. Inert Gas Scattering from Liquid Hydrocarbon Microjets. *J. Phys. Chem. Lett.* **2013**, *4*, 3045−3049.

(25) Artiglia, L.; Edebeli, J.; Orlando, F.; Chen, S.; Lee, M.-T.; Corral Arroyo, P.; Gilgen, A.; Bartels-Rausch, T.; Kleibert, A.; Vazdar, M.; Andres Carignano, M.; Francisco, J. S.; Shepson, P. B.; Gladich, I.; Ammann, M. A Surface-Stabilized Ozonide Triggers Bromide Oxidation at the Aqueous Solution-Vapour Interface. *Nat. Commun.* **2017**, *8*, 700.

(26) Thürmer, S.; Seidel, R.; Faubel, M.; Eberhardt, W.; Hemminger, J. C.; Bradforth, S. E.; Winter, B. Photoelectron Angular Distributions from Liquid Water: Effects of Electron Scattering. *Phys. Rev. Lett.* **2013**, *111*, 173005.

(27) Galinis, G.; Strucka, J.; Barnard, J. C. T.; Braun, A.; Smith, R. A.; Marangos, J. P. Micrometer-Thickness Liquid Sheet Jets Flowing in Vacuum. *Rev. Sci. Instrum.* **2017**, *88*, 083117.
(28) Koralek, J. D.; Kim, J. B.; Brůža, P.; Curry, C. B.; Chen, Z.; Bechtel, H. A.; Cordones, A. A.; Sperling, P.; Toleikis, S.; Kern, J. F.; Moeller, S. P.; Glenzer, S. H.; DePonte, D. P. Generation and Characterization of Ultrathin Free-Flowing Liquid Sheets. *Nat. Commun.* **2018**, *9*, 1353.
(29) Ekimova, M.; Quevedo, W.; Faubel, M.; Wernet, P.; Nibbering, E. T. J. A Liquid Flatjet System for Solution Phase Soft-x-Ray Spectroscopy. *Struct. Dyn.* **2015**, *2*, 054301.
(30) Bush, J. W. M.; Hasha, A. E. On the Collision of Laminar Jets: Fluid Chains and Fishbones. *J. Fluid Mech.* **2004**, *511*, 285−310.
(31) Chen, X.; Ma, D.; Yang, V.; Popinet, S. High-Fidelity Simulations of Impinging Jet Atomization. *Atomization Sprays* **2013**, *23*, 1079−1101.
(32) Atencia, J.; Beebe, D. J. Controlled Microfluidic Interfaces. *Nature* **2005**, *437*, 648−655.
(33) Ismagilov, R. F.; Stroock, A. D.; Kenis, P. J. A.; Whitesides, G.; Stone, H. A. Experimental and Theoretical Scaling Laws for Transverse Diffusive Broadening in Two-Phase Laminar Flows in Microchannels. *Appl. Phys. Lett.* **2000**, *76*, 2376−2378.
(34) Song, H.; Ismagilov, R. F. Millisecond Kinetics on a Microfluidic Chip Using Nanoliters of Reagents. *J. Am. Chem. Soc.* **2003**, *125*, 14613−14619.
(35) Rose, A. L.; Waite, T. D. Chemiluminescence of Luminol in the Presence of Iron(II) and Oxygen: Oxidation Mechanism and Implications for Its Analytical Use. *Anal. Chem.* **2001**, *73*, 5909−5920.
(36) Matsumoto, R.; Yoshida, K.; Matsuo, R. Diffusion in Microchannel Analyzed by Chemiluminescence. *J. Therm. Sci. Technol.* **2013**, *8*, 448−459.
(37) Merenyi, G.; Lind, J.; Eriksen, T. E. The Equilibrium Reaction of the Luminol Radical with Oxygen and the One-Electron-Reduction Potential of 5-Aminophthalazine-1,4-Dione. *J. Phys. Chem.* **1984**, *88*, 2320−2323.
(38) Merényi, G.; Lind, J.; Eriksen, T. E. Luminol Chemiluminescence: Chemistry, Excitation, Emitter. *J. Biolumin. Chemilumin* **1990**, *5*, 53−56.
(39) Merenyi, G.; Lind, J.; Eriksen, T. E. The Reactivity of Superoxide (O2-) and Its Abiulkity to Induce Chemiluminescence with Luminol. *Photochem. Photobiol.* **1985**, *41*, 203−208.
(40) Burdo, T. G.; Seitz, W. R. Mechanism of Cobalt Catalysis of Luminol Chemiluminescence. *Anal. Chem.* **1975**, *47*, 1639−1643.
(41) Gaikwad, A.; Silva, M.; Pérez-Bendito, D. Selective Stopped-Flow Determination of Manganese with Luminol in the Absence of Hydrogen Peroxide. *Anal. Chim. Acta* **1995**, *302*, 275−282.
(42) Ojima, H. In *Advances in Catalytic Activation of Dioxygen by Metal Complexes*; Simándi, L. I., Ed.; Catalysis by Metal Complexes; Springer US, 2002.
(43) Menzi, S.; Knopp, G.; Al Haddad, A.; Augustin, S.; Borca, C.; Gashi, D.; Huthwelker, T.; James, D.; Jin, J.; Pamfilidis, G.; Schnorr, K.; Sun, Z.; Wetter, R.; Zhang, Q.; Cirelli, C. Generation and Simple Characterization of Flat, Liquid Jets. *Rev. Sci. Instrum.* **2020**, *91*, 105109.
(44) O'Sullivan, D. W.; Hanson, A. K.; Kester, D. R. Stopped Flow Luminol Chemiluminescence Determination of Fe(II) and Reducible Iron in Seawater at Subnanomolar Levels. *Mar. Chem.* **1995**, *49*, 65−77.
(45) Steinfeld, J. I.; Francisco, J. S.; Hase, W. L. *Chemical Kinetics and Dynamics*, 2nd ed.; Pearson: Upper Saddle River, N.J, 1998.

https://doi.org/10.1021/jacs.2c01232
J. Am. Chem. Soc. 2022, 144, 7790−7795